Surgical Removal of Visceral Adipose Tissue has Therapeutic Benefit in Male APP^{NL-F} Mice

Samuel A. McFadden[1†], Yimin Fang[1†], Kathleen Quinn[1], Mackenzie R. Peck[1], Jenelle E. Chapman[1], Tiarra Hill[1], Andrzej Bartke[2,3], Erin R. Hascup[1,4], Kevin N. Hascup[1,3,4*]

[1]Dale and Deborah Smith Center for Alzheimer's Research and Treatment, [2]Internal Medicine, [3]Medical Microbiology, Immunology and Cell Biology, and [4]Pharmacology, at Southern Illinois University School of Medicine, Springfield, IL, USA

[†]These authors contributed equally to this work and share first authorship.

*Corresponding Author: Kevin N. Hascup, Dale and Deborah Smith Center for Alzheimer's Research and Treatment, Southern Illinois University School of Medicine, P.O. Box 19628, Springfield, IL 62794-9628, USA Tel: 217-545-6994, Email: khascup49@siumed.edu

Keywords: Alzheimer's disease, lipectomy, white adipose tissue, cell senescence, glucose and lipid metabolism, inflammation, visfatin

Manuscript Length: 5,557 Words

Figures: 7

Tables: 1

Abstract

Purpose: Visceral white adipose tissue (vWAT) accumulation causes systemic inflammation, insulin resistance, metabolic syndrome, and senescent cell accumulation that are risk factors for Alzheimer's disease (AD). Visceral fat removal (VFR) improves metabolism and reduces proinflammatory cytokines. We hypothesized that VFR removal in AD mice would improve metabolism and cognition.

Methods: Male and female APP^{NL-F} mice underwent sham or vWAT surgical resection (epididymal and perirenal) at 4 (pre-symptomatic) and 16 (symptomatic) months of age to understand interventional and therapeutic effects, respectively. At 18 months of age, glucose metabolism and novel object recognition (NOR) memory were assayed followed by assessment of body composition and tissue-specific markers of metabolism, cell senescence, inflammation, or amyloid accumulation.

Results: Male and female APP^{NL-F} mice showed distinct VFR responses. In pre-symptomatic males, increased vWAT lipolysis and hepatic lipogenesis led to ectopic liver lipid accumulation, with reduced adiponectin and leptin, elevated visfatin, and impaired glucose metabolism. Symptomatic males showed reduced vWAT lipogenesis, enhanced hepatic lipolysis, glycolysis, and glycogenesis, lowering liver lipids and improving insulin sensitivity. Only symptomatic males improved NOR, linked to elevated hippocampal learning and memory markers. Female vWAT reaccumulation was due to increased lipogenesis and lower lipolysis. Pre-symptomatic females had lower hepatic lipogenesis, while glycolysis and glycogenesis declined with disease progression. Hippocampal senescence and inflammation were elevated early in the disease that persisted symptomatically.

Conclusions: Sex-specific differences in glucose and lipid metabolism and lipid accumulation underlie the divergent responses to VFR in APP^{NL-F} mice, with symptomatic males showing the only beneficial outcomes in metabolism and cognition.

Graphical Abstract

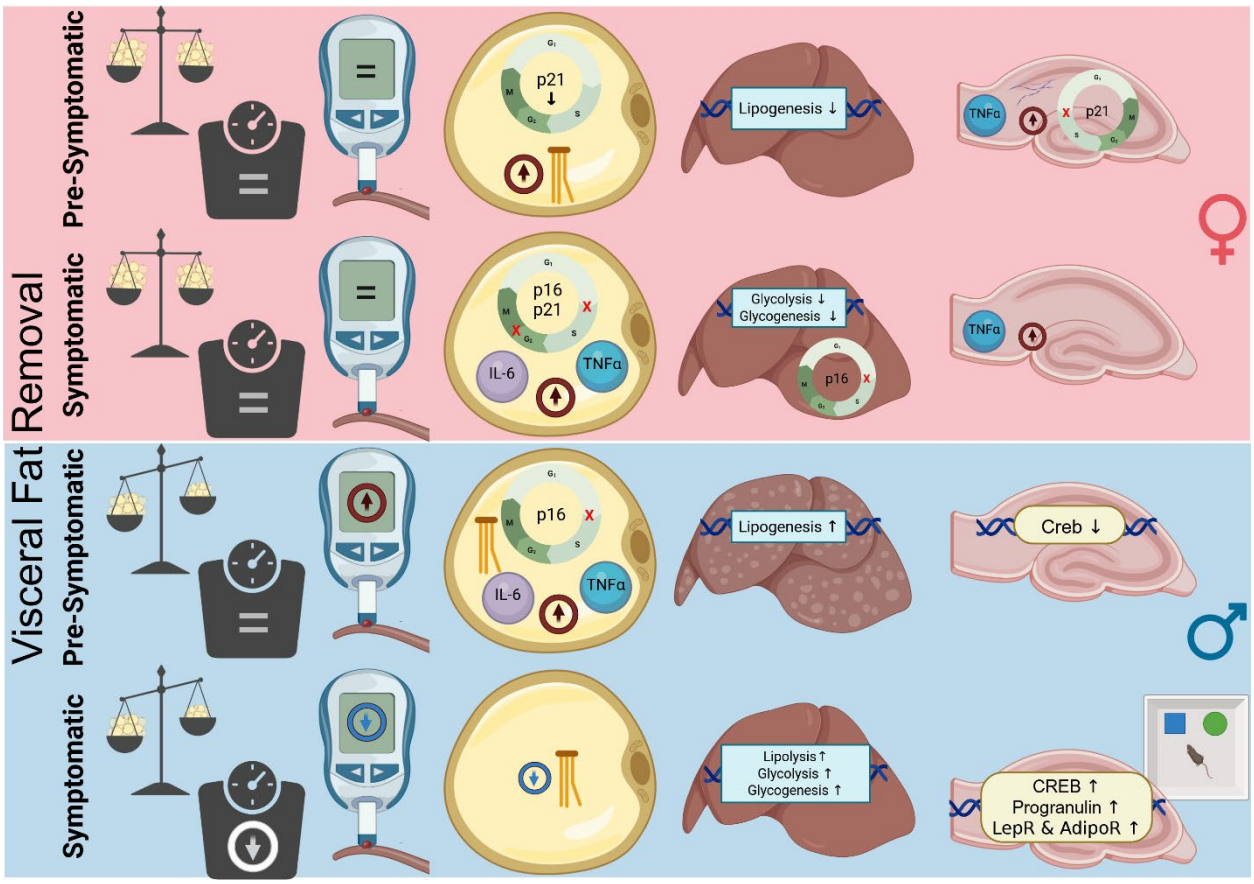

Male and female APP^{NL-F} mice exhibited distinct visceral fat responses to AD progression. In males, early disease stages were marked by vWAT lipolysis and hepatic lipid accumulation with metabolic dysfunction, while symptomatic stages showed a metabolic shift that improved insulin sensitivity and NOR performance. In contrast, females displayed progressive vWAT reaccumulation, reduced hepatic metabolism, and persistent hippocampal senescence and inflammation from early stages onward.

50 **Introduction**

51 Alzheimer's disease (AD) is a progressive, neurodegenerative disorder, and the most prevalent
52 form of dementia. AD is historically characterized by senile plaques composed of aggregated
53 amyloid beta (Aβ) and neurofibrillary tangles formed from hyperphosphorylated tau protein.
54 However, AD is a multifactorial disorder characterized not only by aberrant protein aggregation,
55 but also by mitochondrial dysfunction, oxidative stress, cellular senescence, and chronic
56 inflammation - all of which contribute to disease progression (Breijyeh and Karaman, 2020). The
57 deleterious cascade underlying AD progression is hypothesized to begin in midlife and is not
58 isolated to the CNS. Rather peripheral organs, such as visceral white adipose tissue (vWAT),
59 regulate brain function through hormone secretion as well as glucose and lipid metabolism
60 (Gustafson, 2012, Dove et al., 2021). Accumulation of vWAT in midlife is a predictor for future
61 development of AD (Huang et al., 2022).

62 Adipose tissue regulates many aspects of whole-body physiology, including food intake,
63 maintenance of energy levels, insulin sensitivity, body temperature, and immune responses
64 (Sakers et al., 2022). Adipose tissue is located under the skin (subcutaneous; SubQ), between
65 and around organs (vWAT), interscapular brown adipose tissue (BAT), in bone marrow, and in
66 mammary glands (Wong Zhang et al., 2023). Beyond total adipose tissue mass, the distribution
67 of fat depots is a stronger predictor of obesity-related disease risk and associated complications
68 (Chusyd et al., 2016). Excess vWAT accumulation causes systemic inflammation, insulin
69 resistance, reduced cerebral blood flow, and metabolic syndrome, which contributes to brain
70 volume shrinkage and cognitive decline (Richard et al., 2000, Wong Zhang et al., 2023,
71 Baglietto-Vargas et al., 2016, Biessels and Despa, 2018, Dove et al., 2021, Nguyen et al.,
72 2014).

73 The link between systemic inflammation with vWAT and metabolic dysfunction has been
74 reported in diabetic fatty rodents and in aged rats (Borst et al., 2005, Gabriely et al., 2002,

75 Pitombo et al., 2006). In humans, vWAT is a stronger predictor of age-related cognitive
76 impairment than body mass index (Whitmer et al., 2008, Elias et al., 2005, Kamogawa et al.,
77 2010). A cross-sectional study also showed that vWAT dysfunction and inflammatory status in
78 obesity, is associated with increased cerebral Aβ burden in midlife (Kim et al., 2022).
79 Transplantation of vWAT from obese mice led to impaired cognition in lean wild-type recipient
80 mice mediated by NLRP3/IL-1β signaling (Guo et al., 2020). Removal of vWAT prevented
81 obesity-induced insulin resistance, hyperinsulinemia, and decreased plasma proinflammatory
82 cytokine levels (Borst et al., 2005, Gabriely et al., 2002, Pitombo et al., 2006), which improved
83 glucose metabolism (Barzilai et al., 1999, Foster et al., 2011, Franczyk et al., 2021). Aging also
84 increases vWAT senescent cell burden leading to a chronic pro-inflammatory state (Tchkonia et
85 al., 2010). Reduction of senescent cells in vWAT improves metabolic and cognitive performance
86 in normal aging (Fang et al., 2023) and AD mice (Fang et al, 2025).

87 Considering the contribution of vWAT accumulation on cognitive decline and AD progression,
88 we hypothesized that surgical resection of this adipose depot would improve the metabolic
89 profile and reduce cognitive impairments in the APP^{NL-F} AD mouse model. APP^{NL-F} mice contain
90 the human Aβ isoform of the Swedish (KM670/671NL) and Iberian (I716F) mutations knocked
91 into the *App* locus leading to upregulation of $A\beta_{42}$ without overexpression of APP (Saito et al.,
92 2014, Benitez et al., 2021). Plaque accumulation begins at ~6 months of age while cognitive
93 impairments occur between 12-18 months of age. Our prior research indicates that both sexes
94 of APP^{NL-F} mice have increased markers of senescent cell ($p16^{Ink4\alpha}$ and $p21^{Cip1}$) and
95 senescence-associated secretory phenotype (SASP; IL-6, TNFα, MIP1α) in vWAT by four
96 months of age (Fang et al., 2025). To test our hypothesis, we surgically resected vWAT
97 (epididymal and perirenal) from male and female APP^{NL-F} mice at either 4 or 16 months of age.
98 These time points allowed us to examine the effects of visceral fat removal (VFR) for pre-
99 symptomatic intervention (4 months) or symptomatic therapy (16 months). All metabolic and

100 cognitive assays were conducted at 18 months of age. Our results indicate that VFR effects
101 were disease stage- and sex-dependent with metabolic and cognitive benefits observed in
102 symptomatic male APP^{NL-F} mice.

Material and Methods

Chemicals

All chemicals were stored according to manufacturer recommendations unless stated otherwise. The Phosphovanilin (PV) reagent for lipid determination was prepared by using six milligrams of vanillin (Fisher Scientific Cat # AC140821000) dissolved in 100 mL of 37°C water and further diluted to 500 mL with 85% phosphoric acid.

Animals

Founder APP^{NL-F} mice on a C57BL/6 background (RRID: IMSR_RBRC06343) were obtained from Riken (Japan). C57BL/6 (RRID:IMSR_JAX:000664) mice were originally obtained from The Jackson Laboratory (Bar Harbor, ME) and used to maintain the genetic background of the breeding colonies. At weaning, pups were randomly assigned to mixed-litter cages and group-housed with mice of the same sex and genotype to control for litter size, maternal care, and other potential litter-specific variables. Protocols for animal use were approved by the Institutional Animal Care and Use Committee at Southern Illinois University School of Medicine (Protocol number: 2025-055), which is accredited by the Association for Assessment and Accreditation of Laboratory Animal Care. All studies were conducted in accordance with the United States Public Health Service's Policy on Humane Care and Use of Laboratory Animals. Mice were group housed on a 12:12 h light-dark cycle, with food (Chow 5001 with 23.4% protein, 5% fat, and 5.8% crude fiber; LabDiet PMI Feeds) and water available ad libitum. Genotypes were confirmed by collecting a 5 mm tail tip for DNA analysis by TransnetYX, Inc (Cordova, TN).

Visceral Fat Removal (VFR) Surgery

Four and sixteen-month-old male and female APP^{NL-F} mice were randomized into two groups – VFR (epidydimal and perirenal) and sham-operated. Mice were isoflurane anesthetized,

127 abdominal fur shaved, and betadine scrubbed over the incision site. An ~1.5 cm vertical midline
128 incision along the lower abdomen in males or ventral incisions on either lateral abdominal side
129 in females were made to access epidydimal adipose depots. The perinephric adipose depots
130 were removed by flank incisions. Adipose depots were removed by blunt dissection. Mice that
131 underwent the sham operation had their vWAT mobilized, but not removed. Absorbable sutures
132 were used to close the body cavity while wound clips were used on the skin. Tylenol (1 mg/mL)
133 was administered in the drinking water from one day pre- to 3 days post-surgery.

134 Glucose tolerance test (GTT) and insulin tolerance test (ITT)

135 Glucose metabolism was assessed via GTT and ITT when mice reached 18 months of age (14
136 or 2 months post VFR surgery) as previously described (Fang et al., 2023). Fifteen-hour-fasted
137 mice underwent GTT by intraperitoneal (i.p.) injection with 2.0 g glucose per kg of body weight
138 (BW). Blood glucose levels were measured at 0, 15, 30, 45, 60, and 120 min with a PRESTO
139 glucometer (AgaMatrix). For ITT, mice were injected i.p. with 1 IU porcine insulin from sigma
140 (St. Louis, MO) (Cat# I5523) per kg of BW. Blood glucose levels were measured at 0, 15, 30,
141 45, 60, and 120 min.

142 Novel object recognition (NOR) task

143 The NOR was used to evaluate memory retention based on the premise that mice spend more
144 time exploring a novel object rather than a familiar object if the animal remembers the familiar
145 object. Mice were habituated in the open field chamber for 30 min on the first day. Twenty-four
146 hours after, the mouse was returned to the chamber and presented with two similar objects for 5
147 min. A 24 hr inter-session-interval was used between introduction and retention phases to
148 promote long-term memory retrieval. During the retention phase one of the familiar objects was
149 replaced with a novel object and the mouse was given 5 minutes of exploration. The ANY-maze
150 video tracking system (Stoelting Co., Wood Dale, IL) was used to record mouse navigation

151 during the familiarization and retention phases and used to calculate the retention index and
152 novelty preference.

153 Body composition and tissue procurement

154 At 19 months of age, body weight was recorded and mice were anesthetized using isoflurane.
155 A cardiac puncture was used to collect the plasma. The blood was mixed with EDTA, followed
156 by centrifugation at 10,000 g for 15 min at 4°C for plasma collection. Immediately following
157 cardiac puncture, mice were decapitated and the peripheral tissues (liver, pancreas,
158 perigonadal and subcutaneous (SubQ) WAT, and BAT) were weighed to calculate their
159 contribution to total body weight. Tissue was immediately flash frozen and stored at -80˚C until
160 processing as previously described (Fang et al., 2023).

161 Total Liver Lipid Quantification

162 A modified micro-scale colorimetric sulfo-phospho-vanillin (SPV) method was used to measure
163 total liver lipids (Tran et al., 2019). Approximately 50 mg of liver tissue was homogenized in
164 1000 µL of chloroform/methanol (2:1) followed by addition of 500 µL of saline. The mixture was
165 vortexed then centrifuged at 10,000 rpm for 5 minutes. The chloroform layer was separated and
166 evaporated at 90°C for ~20 min, then incubated at 90°C with 200 µL of 98% sulfuric acid for 20
167 min. After adding 750 µL of vanillin–phosphoric acid reagent, samples were incubated at 37˚C
168 for 15 min, cooled to 25˚C, and 200 µL was transferred to a 96-well microplate. Absorbance was
169 measured at 530 nm, and lipid content was normalized to tissue weight.

170 Assessment of blood chemistry

171 Per the manufacturer's protocol, adiponectin or leptin was measured with respective ELISA kits
172 from Crystal Chem (Elk Grove Village, IL; Cat# 80569, 90030). Visfatin was measured by an
173 ELISA kit from Mybiosource (San Diego, CA; Cat# MBS760980).

174 RT–PCR

175 mRNA expression was analyzed by quantitative RT–PCR as previously described (Fang et al.,
176 2020) using Bio-Rad cDNA synthesis kits (Cat # 1708897 and 1708891) and SYBR green mix
177 (Cat # 1725121) and the QuantStudio 3 Real-Time PCR (Thermo Fisher Scientific). RNA was
178 extracted using a RNeasy mini kit or RNeasy Lipid Tissue Mini Kit (Qiagen) following the
179 manufacturer's instructions. Relative expression was calculated as previously described
180 (Masternak et al., 2012) and primers were purchased from Integrated DNA Technologies. A list
181 of forward and reverse primers used in this study is shown in Table 1.

182 Soluble $A\beta_{42}$ Quantification

183 The hippocampus from one hemisphere was dissected and stored at -80°C until tissue
184 processing. Soluble $A\beta_{42}$ concentrations were determined using the Human / Rat β amyloid
185 ELISA kits (WAKO Chemicals; Cat: 290-62601) according to the manufacturer recommended
186 protocols.

187 Statistical analysis

188 Statistical analyses were conducted to determine differences between age- and sex-matched
189 sham and VFR groups using unpaired two-tailed Student's t tests with significance defined as p
190 < 0.05. Data are presented as mean ± SEM. All statistical analyses and graphs were completed
191 using Prism 10 (GraphPad Inc, La Jolla, CA, USA).

192 **Results**

193 VFR at the symptomatic time point improved object recognition memory in male APP^{NL-F} mice.

194 To explore whether VFR could improve object recognition memory in APP^{NL-F} mice, surgery was
195 performed at a pre-symptomatic stage (4 months of age, prior to detectable plaque
196 accumulation and cognitive decline) or a symptomatic stage (16 months of age, during
197 advanced pathology and functional decline). Both male and female APP^{NL-F} cohorts were
198 included to assess sex-specific effects of VFR. Object recognition memory was assayed at 18
199 months of age via the NOR task. Only male APP^{NL-F} mice with VFR surgery at the symptomatic
200 time point had improved recognition memory as indicated by increased retention index (Fig. 1A)
201 and novelty preference (Fig. 1B) compared to the age- and sex-matched sham surgery controls.
202 VFR surgery performed at the pre-symptomatic time point in male, or either time point of female
203 APP^{NL-F}, had no effect on object recognition memory (Fig 1A-B).

204 VFR resulted in changes to body weight and composition in an age- and sex-dependent
205 manner.

206 To assess physiological changes caused by VFR, we examined body composition at ~19
207 months of age upon euthanization. Symptomatic male APP^{NL-F} mice with VFR had decreased
208 BW compared to the sham group (Fig 1C). No differences were observed in the other VFR
209 groups. The body composition analyses indicated that after VFR, vWAT accumulated in all
210 ages and sexes but at different percentages. Female VFR APP^{NL-F} mice had vWAT
211 reaccumulation occurring in 92% and 100% of mice in the pre-symptomatic and symptomatic
212 cohorts, respectively (Fig. 1D). In contrast, ~50% of the male mice with VFR surgery at either
213 age observed vWAT reaccumulation (Fig. 1D). This difference in vWAT was the major
214 contributor to the observed changes of total percent adipose mass when including SubQ,

215 interscapular BAT, and vWAT (Fig. 1E). In summary, the body weight of symptomatic VFR male
216 APP^{NL-F} mice was reduced mainly due to less vWAT reaccumulation.

217 <u>VFR during the pre-symptomatic time point in male APP^{NL-F} mice caused ectopic liver lipid</u>
218 <u>deposition via increased de novo lipogenesis.</u>

219 Although reduced reaccumulation of vWAT was similar between pre-symptomatic and
220 symptomatic VFR male APP^{NL-F} mice, surgery at the pre-symptomatic time point did not affect
221 BW. Body composition changes without effects on BW are known to happen with aging (St-
222 Onge and Gallagher, 2010). We sought to identify tissue composition changes that caused the
223 increased body weight despite reduced adiposity in the pre-symptomatic VFR male mice.
224 Lipodystrophy leads to the excessive deposition of lipids in other organs, such as the liver,
225 contributing to insulin resistance (Petersen and Shulman, 2018). To test whether the liver had
226 more ectopic fat deposition, the percentage of total liver lipids was measured. Pre-symptomatic
227 VFR male APP^{NL-F} mice had a higher percentage of liver lipids compared with sham controls
228 (Fig 2A). In symptomatic APP^{NL-F} VFR male mice, total liver lipids were reduced compared with
229 sham surgery controls while no differences were observed in females at either disease stage.

230 Liver gene expression showed that key *de novo* lipogenesis genes including acetyl-coenzyme A
231 carboxylase (ACC), fatty acid synthase (FAS), stearoyl-CoA desaturase 1 (SCD1), elongation of
232 long-chain fatty acids family member 6 (Elovl6), sterol regulatory element-binding protein-1
233 (SREBP1) were increased in pre-symptomatic VFR male APP^{NL-F} mice compared with sham
234 controls (Fig 2B). In pre-symptomatic VFR female APP^{NL-F} mice, expression of these same
235 genes (except for ACC) were decreased. Interestingly, liver gene expression of monoglyceride
236 lipase (MGL), the rate-limiting enzyme in lipolysis, was upregulated only in symptomatic VFR
237 male APP^{NL-F} mice (Fig. 2B). This is one explanation for the decreased BW and vWAT observed
238 in this group. These data indicated that pre-symptomatic VFR male APP^{NL-F} mice accumulated

239 more ectopic liver lipids likely due to higher *de novo* lipogenesis, while the contrary was
240 observed in symptomatic males due to higher lipolysis.

241 VFR in female APP^{NL-F} mice led to increased gene expression of de novo lipogenesis and
242 decreased expression of lipolysis genes in reaccumulated vWAT.

243 Nearly all the VFR APP^{NL-F} female mice reaccumulated vWAT to levels observed in sham
244 surgery controls matched for age and sex (Fig. 1D). To understand the reason for this
245 reaccumulation, we examined gene expression of lipogenesis and lipolysis in vWAT (Fig 2C).
246 Expression levels of two key *de novo* lipogenesis genes, ACC and FAS, were increased in VFR
247 APP^{NL-F} female mice at either disease stage. The expression of ACC and FAS were decreased
248 in VFR male APP^{NL-F} mice at the symptomatic, but not at the pre-symptomatic time point.
249 Lipolysis gene expression, including protein kinase A (PKA), adipocyte triglyceride lipase
250 (ATGL), and hormone sensitive lipase (HSL), were decreased at both disease stages in VFR
251 APP^{NL-F} female mice compared with sham controls. In male mice, expression of PKA, ATGL,
252 and HSL were increased at the pre-symptomatic, but unchanged, at the symptomatic time point.
253 The data suggests that the accumulation of vWAT after VFR in female APP^{NL-F} mice at either
254 stage of disease progression is a result of increased lipogenesis and decreased lipolysis gene
255 expression. In male APP^{NL-F} mice, the reduced accumulation of vWAT after VFR was disease
256 stage specific with pre-symptomatic time points increasing expression of lipolysis genes, while
257 surgery at the symptomatic time point decreased lipogenesis gene expression. Interestingly,
258 SREBP1 vWAT expression was upregulated only in VFR APP^{NL-F} male mice during the pre-
259 symptomatic time point. SREBP1 is a transcription factor activated by high blood glucose
260 (Bertolio et al., 2019, Zhao et al., 2024), suggesting altered glucose metabolism in this cohort.

261 VFR surgery impacted either glucose tolerance or insulin sensitivity in male APP^{NL-F} mice.

262 Lipid metabolism plays an important role in regulating glucose utilization, and the two processes
263 are tightly interconnected (Parhofer, 2015). Accordingly, the observed changes in lipid
264 metabolizing gene expression could affect glucose metabolism. To test the effects of VFR on
265 blood glucose metabolism, we monitored fasting and fed glucose levels as well as glucose
266 tolerance with a GTT, and insulin sensitivity with an ITT, at 18 months of age. Pre-symptomatic
267 VFR APP^{NL-F} male mice were less glucose tolerant, but no effects were observed in
268 symptomatic males (Fig 3A). Insulin sensitivity was improved in symptomatic VFR APP^{NL-F} male
269 mice, but differences were not observed in pre-symptomatic males (Fig 3B). Consistent with the
270 GTT, fasting glucose was higher in pre-symptomatic VFR APP^{NL-F} male mice compared with
271 sham controls (Fig. 3C). No fasting glucose changes were observed in symptomatic APP^{NL-F}
272 male mice, nor were differences in fed glucose observed (Fig. 3D) in either male cohort. No
273 blood glucose differences were observed at either disease stage in VFR APP^{NL-F} female mice.

274 The liver plays a major role in the control of whole body glucose homeostasis (Han et al., 2016,
275 Guerra and Gastaldelli, 2020, Scoditti et al., 2024). To understand the observed blood glucose
276 differences, we examined liver gene expression (Fig 4A) associated with gluconeogenesis
277 (synthesis of glucose from non-carbohydrate sources), glycolysis (breakdown of glucose for
278 energy), and glycogenesis (conversion of glucose to glycogen). Expression of gluconeogenesis
279 genes, glucose-6-phosphatase (G6PC) and phosphoenolpyruvate carboxykinase (PEPCK),
280 were increased in pre-symptomatic VFR APP^{NL-F} male mice, which was consistent with their
281 increased fasting blood glucose levels (Fig 3C). In contrast, glucose transporter 2 (Glut2), GCK
282 (Glucokinase), and glycogen synthase 2 (GYS2), key genes in glycolysis and glycogenesis,
283 respectively, were increased in male, but decreased in female APP^{NL-F} mice after symptomatic
284 VFR.

285 Taken together, the blood glucose and liver gene expression measures indicate VFR affected
286 glucose metabolism in a sex- and disease stage-dependent manner. Pre-symptomatic VFR in

287 APP^{NL-F} male mice increased their fasting blood glucose and made them less glucose tolerant,
288 likely mediated via increasing gluconeogenesis. At symptomatic time points, VFR improved
289 glucose metabolism by increasing insulin sensitivity via enhancing glycolytic and glycogenesis
290 gene expression. Although this gene expression was reduced in symptomatic VFR female
291 mice, no effects on insulin sensitivity or blood glucose levels were observed.

292 <u>VFR alters plasma visfatin, adiponectin, and leptin in pre-symptomatic male APP^{NL-F} mice.</u>

293 Adipokines secreted from adipose tissue are important for whole-body glucose metabolism and
294 insulin sensitivity (Rabe et al., 2008, Kojta et al., 2020). Given the altered lipid and glucose
295 metabolism after VFR in the APP^{NL-F} mice, we examined plasma adipokines. Visfatin is
296 primarily produced in vWAT, with plasma levels increasing in response to high-fat diet feeding
297 and obesity (Adeghate, 2008, Sethi and Vidal-Puig, 2005), and is associated with glucose
298 intolerance (Abdalla, 2022). Plasma visfatin was increased in pre-symptomatic VFR male
299 APP^{NL-F} mice compared with age-matched sham controls (Fig 4B), consistent with their higher
300 ectopic liver accumulation, fasting blood glucose, and glucose intolerance. No plasma visfatin
301 differences were observed in the other mouse cohorts.

302 Adiponectin enhances glucose and lipid metabolism (Yanai and Yoshida, 2019), decreases
303 lipogenesis (Richard et al., 2000), and has neuroprotective effects (Khoramipour et al., 2021).
304 Plasma adiponectin was reduced in pre-symptomatic VFR APP^{NL-F} male mice (Fig 4C). This
305 would also contribute to the reduced glucose metabolism and increased liver lipid observed in
306 this cohort. Plasma adiponectin changes were not observed after VFR in the other cohorts.

307 Leptin regulates appetite and energy expenditure, and its deficiency can disrupt glucose and
308 lipid metabolism, leading to neuronal damage that impairs neuroplasticity and memory
309 consolidation (Fernandes et al., 2024). Higher leptin levels are also associated with a lower
310 dementia risk (Lieb et al., 2009). Plasma leptin was decreased in pre-symptomatic VFR APP^{NL-F}

311 male mice compared with age-matched sham controls (Fig. 4D), which contributed to the
312 imbalance of glucose and lipid metabolism in this male cohort. Differences in plasma leptin
313 levels were not observed in the other cohorts of mice.

314 VFR increases WAT senescent cell and SASP markers in pre-symptomatic male and
315 symptomatic female APP^{NL-F} mice.

316 Adipose tissue, particularly vWAT, has the highest burden of senescent cells (Palmer et al.,
317 2021) and we previously showed senescent cell markers in vWAT were increased in male and
318 female APP^{NL-F} mice (Fang et al., 2025). VFR can decrease systemic and neuroinflammation in
319 aged mice (Shin et al., 2015). We examined gene expression of senescent cell and SASP
320 markers in vWAT (Fig 5A). In pre-symptomatic VFR APP^{NL-F} male mice, gene expression of
321 $p16^{Ink4\alpha}$, $p21^{Cip1}$, and IL-10 were increased in vWAT. Expression of vWAT $p16^{Ink4\alpha}$ and TNFα
322 were also increased in symptomatic VFR APP^{NL-F} female mice (Fig 5A) while no differences in
323 IL-6 and MCP1 were observed in any cohort (data not shown). SASP markers were also
324 examined in SubQ WAT where TNFα, IL-10, IL-6, and MCP1 were all increased in pre-
325 symptomatic VFR APP^{NL-F} male mice (Fig 5B). SubQ IL-6 was also increased in symptomatic
326 VFR APP^{NL-F} female mice. Overall, VFR increased gene expression of senescent cell and
327 SASP markers in WAT of pre-symptomatic APP^{NL-F} male mice, with a modest increase
328 observed in symptomatic females.

329 VFR modulates gene expression of hippocampal senescence, SASP, and cognitive markers.

330 Excess vWAT accumulation is linked to accelerated brain aging, neuroinflammation, and
331 dementia risk (Moser and Pike, 2016, Oh et al., 2023, Budamagunta et al., 2023). To
332 understand how VFR affected hippocampal function, the brain region strongly associated with
333 learning and memory, we examined gene expression of cell senescence and cytokines (Fig 6A).
334 VFR had no effect on $p16^{Ink4\alpha}$, $p21^{Cip1}$, or TNFα expression in APP^{NL-F} male mice at either stage

335 of disease progression. Alternatively, p16$^{Ink4\alpha}$ gene expression was increased in symptomatic
336 VFR APP^{NL-F} female mice. There was a corresponding increase in TNFα expression in this
337 cohort as well as the symptomatic females. VFR had deleterious effects on hippocampal
338 senescence and inflammation in female, but not male APP^{NL-F} mice.

339 Since we observed improvements in object recognition memory after VFR in symptomatic male
340 APP^{NL-F} mice, we examined markers associated with learning and memory in the hippocampus
341 (Fig 6A). Both adiponectin and leptin receptors (AdipoR, LepR) are found in the hippocampus
342 and play a role in synaptic plasticity and cognition. Gene expression of both receptors were
343 upregulated in symptomatic VFR APP^{NL-F} male mice (Fig 6A). In females, VFR increased LepR
344 in the pre-symptomatic disease stage. Cyclic AMP response element-binding protein 1 (Creb1),
345 plays a role in long-term memory formation. Creb1 gene expression was decreased in pre-
346 symptomatic VFR APP^{NL-F} male mice, but elevated in the symptomatic male cohort. Progranulin
347 (PRGN) is important for neuronal survival and growth in the hippocampus. PRGN gene
348 expression was decreased in pre-symptomatic VFR APP^{NL-F} female mice, but increased in
349 symptomatic males. Overall, VFR altered the hippocampal gene expression profile of
350 symptomatic APP^{NL-F} male mice in a manner that would improve their object recognition
351 memory.

352 <u>Soluble Aβ_{42} is increased in pre-symptomatic male and female mice.</u>

353 Soluble Aβ_{42} is the neurotoxic species associated with synaptic dysfunction and cognitive
354 decline in AD (Findley et al., 2019). An ELISA indicated hippocampal soluble Aβ_{42} (Fig 6B)
355 production was increased in VFR APP^{NL-F} male and female mice, but only during the pre-
356 symptomatic disease stage. VFR during the symptomatic stage had no effect on soluble Aβ_{42}.

357 **Discussion**

358 Adipose accumulation and distribution differ between sexes and are evolutionarily conserved.
359 Females typically have a higher overall fat percentage with a large proportion stored
360 subcutaneously for energy supply during pregnancy and lactation during food scarcity, while
361 males accumulate fat in visceral regions. Numerous variables influence adipose development
362 including sex chromosomes, gonadal hormone levels, and hormone receptors. Sex
363 chromosome complement impacts adipose accumulation whereby the presence of two "X"
364 chromosomes leads to higher accumulation while the presence of the "Y" chromosome has no
365 influence. The gonadal hormones, testosterone and estrogen, drive visceral and subcutaneous
366 adipose accumulation in males and females, respectively. Age-related hormonal changes
367 increase vWAT accumulation regardless of sex and is a key factor in the development of
368 metabolic syndrome that increases dementia risk.

369 Besides its role as an energy reservoir, adipose tissue is an endocrine organ that secretes
370 peptides such as TNFα, IL-6, and adiponectin, which can influence either tissue-specific or
371 whole body metabolism. Prior studies examining VFR effects in rodents were conducted to
372 elucidate mechanisms contributing to metabolic improvements. VFR improves insulin sensitivity
373 and glucose tolerance in young, aged, and obese rodents with some of the metabolic changes
374 occurring through decreased free fatty acids, leptin, and TNFα expression (Kim et al., 1999,
375 Gabriely et al., 2002, Shi et al., 2007a). VFR in aged C57BL/6 mice led to reduced expression
376 of proinflammatory cytokines in the plasma, WAT, and cortex (Shin et al., 2015). Although
377 adiponectin plays a key role in glucose and lipid metabolism and suppresses inflammatory
378 cytokines, serum levels are found to decrease following VFR in male and female Sprague
379 Dawley rats (Borst et al., 2005, Ling et al., 2014), which may be due to the absence of these
380 WAT depots after VFR. Considering the metabolic benefits of VFR and the known link between
381 metabolic dysfunction and AD risk, we aimed to investigate the impact of VFR in an AD model.

382 Prior research has shown APP^{NL-F} mice, particularly females, have worse glucose tolerance
383 (Abi-Ghanem et al., 2025), potentially due to increased senescent cell and SASP markers in
384 vWAT (Fang et al., 2025). Senescent adipocytes contribute to chronic systemic inflammation
385 and metabolic dysfunction, which diminishes cognitive reserve, promotes the accumulation of
386 misfolded proteins, and accelerates AD progression (Huang et al., 2022). We hypothesized that
387 surgical resection of vWAT would improve metabolic function and recognition memory in APP^{NL-}
388 ^{F} mice. We performed VFR at two different stages of disease progression to explore
389 interventional and therapeutic strategies.

390 Surprisingly, the VFR response was disease stage- and sex-dependent. The removal of vWAT
391 in symptomatic APP^{NL-F} male mice improved object recognition memory potentially due to
392 increased hippocampal AdipoR, LepR, Creb1, and PRGN expression. Lipogenesis vWAT gene
393 expression was down-regulated, while hepatic genes associated with lipolysis, glycolysis, and
394 glycogenesis were up-regulated. These effects were associated with a decreased percentage
395 of total liver lipids. All of these alterations were reflected by a reduced percentage of total fat,
396 specifically reaccumulated vWAT, BW, and improved blood glucose maintenance. The opposite
397 was true for VFR during the pre-symptomatic stage in males. After VFR, an imbalance of lipid
398 metabolism was prevalent, reflected by an elevated expression of vWAT lipolysis and hepatic
399 lipogenesis genes. This tissue metabolic imbalance accounts for the redistribution of lipids into
400 other organs, such as the liver, where higher ectopic fat accumulation was observed. Plasma
401 adiponectin and leptin were decreased along with increased visfatin resulting in impaired
402 glucose metabolism and peripheral inflammation. Reduced hippocampal Creb1 expression and
403 increased soluble $A\beta_{42}$, combined with the aforementioned adverse physiological changes,
404 failed to improve object recognition memory.

405 In contrast to males, vWAT reaccumulated in nearly all female mice regardless of when VFR
406 occurred, attributed to higher lipogenesis and lower lipolysis gene expression. Although ectopic

407 lipid deposition did not accumulate in the liver, VFR in pre-symptomatic female APP^{NL-F} mice led
408 to decreased hepatic lipogenesis gene expression, while expression of genes involved in
409 glycolysis and glycogenesis were decreased in symptomatic females. These results were in
410 opposition to age-matched males. Hippocampal soluble $A\beta_{42}$, senescent cell, and inflammatory
411 markers were elevated in pre-symptomatic APP^{NL-F} female mice while the later was only
412 observed at the symptomatic time point. No changes to blood glucose levels or object
413 recognition memory were observed in females after VFR.

414 Lipectomy in mice, rats, and other small mammals does not result in long-term BW loss with
415 regain occurring 12-14 weeks post-surgery (Murillo et al., 2019). In the majority of the studies
416 this was attributed to regeneration of the lipectomized depot, redistribution of fat to other
417 adipose depots, or ectopic fat accumulation in other organs. In our present study, female APP^{NL-}
418 ^{F} mice regained BW due to accumulating vWAT. Although vWAT accumulation was lower in
419 pre-symptomatic males, they regained BW due to ectopic fat distribution in the liver. Only
420 symptomatic APP^{NL-F} male mice had lower BW attributed to less visceral adiposity.
421 Redistribution of fat to other adipose depots was not observed in any cohort. Our present study
422 was designed to examine disease stage-specific interventional or therapeutic AD strategies
423 rather than examining the contribution of aging on adiposity and AD progression. Regardless,
424 effects of aging on adipose accumulation likely contributed to the observed differences in lipid
425 distribution and the comparable end-of-study BW between sham and VFR cohorts matched for
426 age and sex. Estropause and the gradual decrease in estrogen levels that favors vWAT rather
427 than SubQ accumulation may partially account for visceral accumulation after resection in
428 female mice, while in males, ectopic liver lipid distribution has been observed with aging
429 (Donato et al., 2014).

430 The exact mechanisms behind this adipose rebound are not well known, but suggest biological
431 feedback systems that act to preserve energy balance. For example, the adipostat hypothesis

postulates that alterations to energy reserves triggers compensatory mechanisms in metabolism and/or thermogenesis to restore the reservoir. Since gonadal hormones and sex chromosome complement mediate adipose storage, distribution, and utilization, male and female mice use different behavioral strategies to restore fat after lipectomy. Males increase caloric consumption while females reduce heat production and energy expenditure (Shi et al., 2007b). Our findings are in support of this whereby pre-symptomatic VFR APP^{NL-F} male mice had increased gluconeogenesis gene expression and fasting blood glucose, and worse glucose tolerance. Female VFR APP^{NL-F} mice had reduced glycolysis and lipolysis, but increased lipogenesis gene expression. It is important to note, however, that our study was not intended to serve as a preclinical model for liposuction, as that procedure primarily targets SubQ rather than vWAT depots. However, lipectomy in humans causes a transient decrease in body fat and weight that gradually return to preoperative levels within months (Hernandez et al., 2011, Seretis et al., 2015), suggesting the preservation of this energy balance is conserved across species.

The accumulation of WAT and subsequent increases in BW begins in midlife and continues into early aging in both humans (40-65 years) and mice (12-18 months). The reason for this increase is attributed to adipogenesis and adipocyte hypertrophy that are prominent during midlife (Wang et al., 2025). Remodeling of vWAT, like its distribution, varies between sexes, with estrogen levels playing a key role in regulating these processes and shifting notably with age. Female mice have increased adipose progenitor cells leading to hyperplasia while males experience hypertrophy (Wu et al., 2017). Both increase adipose accumulation, but hyperplasia is associated with better metabolic health (Steiner and Berry, 2022), which may explain why blood glucose levels were unaffected in female mice after VFR. Hypertrophic adipocytes secrete less adiponectin and release more proinflammatory cytokines with the latter causing ectopic lipid distribution into other organs, which were all prevalent in pre-symptomatic VFR

456 APP^{NL-F} male mice. Accordingly, adipose cell size rather than number correlates with increased
457 risk for metabolic syndrome (Vishvanath and Gupta, 2019).

458 Senescent cell accumulation in both the periphery and brain contribute to aging and age-related
459 neurodegenerative disorders such as AD. The mechanisms behind this are multifaceted and
460 dependent upon the type of senescent cell (Zhu et al., 2024). Senescent brain cells alter
461 amyloid precursor protein (APP) processing by shifting it from the non-amyloidogenic to the
462 amyloidogenic pathway, promoting the formation of Aβ (Sun et al., 2018). The proinflammatory
463 SASP response coupled with decreased microglial phagocytosis of misfolded proteins can lead
464 to the subsequent Aβ accumulation and deposition in the brain. We observed elevated
465 hippocampal soluble $A\beta_{42}$ in pre-symptomatic VFR APP^{NL-F} mice compared with sex-matched
466 sham controls. Senescent cell and SASP accumulation were prevalent in the WAT of pre-
467 symptomatic males, while these were increased in the hippocampus of pre-symptomatic
468 females. In AD mouse models, reducing peripheral and hippocampal senescent cell burden with
469 senolytics has been shown to reduce amyloid pathology and improve cognitive performance -
470 albeit with benefits favoring female mice (Currais et al., 2014, Zhang et al., 2019, Fang et al.,
471 2025, Ng et al., 2024).

472 Given that AD pathology is thought to initiate in midlife prior to cognitive decline, the concurrent
473 increase in adipose tissue accumulation during this period may play a causal role in disease
474 progression. Our present study indicates accumulation or redistribution of adipose tissue during
475 the pre-symptomatic AD stage can cause metabolic disturbances resulting in sex-specific
476 peripheral and cerebral senescent cell accumulation that exacerbates pathological AD
477 progression. However, during symptomatic AD stages, elimination of vWAT has beneficial
478 metabolic and cognitive effects in male, but not female APP^{NL-F} mice. These sex-specific
479 differences are attributed to increasing energy storage in female symptomatic mice.

480

481 **Disclosures**

482 The authors state that they have no financial or non-financial competing interests to disclose.
483 SAM, YF, MRP, KQ, TH, and JEC conducted the experiments and analyzed the data. YF, AB,
484 KNH, and ERH conceived the study, designed the experiments, interpreted the data, and wrote
485 the manuscript. All authors approved the final version of the manuscript.

486

487 **Funding Sources**

488 This work was supported by the National Institutes of Health NIA R01-AG057767 and NIA R01-
489 AG061937, Kenneth Stark Endowment, and Dale and Deborah Smith Center for Alzheimer's
490 Research and Treatment (YF, MRP, KQ, JEC, SM, TH, KNH, ERH). Geriatrics Initiative (AB).

491

492 **References**

493 ABDALLA, M. M. I. 2022. Role of visfatin in obesity-induced insulin resistance. *World J Clin Cases,* 10**,**
494 10840-10851.
495 ABI-GHANEM, C., KELLY, R. D., GROOM, E. A., VALERIAN, C. G., PAUL, A. S., THRASHER, C. A., SALINERO,
496 A. E., BATCHELDER, M. R., LAFRICAN, J. J., WANG, M., SMITH, R. M., TEMPLE, S., ZULOAGA, D. G.
497 & ZULOAGA, K. L. 2025. Interactions between menopause and high-fat diet on cognition and
498 pathology in a mouse model of Alzheimer's disease. *Alzheimers Dement,* 21**,** e70026.
499 ADEGHATE, E. 2008. Visfatin: structure, function and relation to diabetes mellitus and other
500 dysfunctions. *Curr Med Chem,* 15**,** 1851-62.
501 BAGLIETTO-VARGAS, D., SHI, J., YAEGER, D. M., AGER, R. & LAFERLA, F. M. 2016. Diabetes and
502 Alzheimer's disease crosstalk. *Neurosci Biobehav Rev,* 64**,** 272-87.
503 BARZILAI, N., SHE, L., LIU, L., WANG, J., HU, M., VUGUIN, P. & ROSSETTI, L. 1999. Decreased visceral
504 adiposity accounts for leptin effect on hepatic but not peripheral insulin action. *Am J Physiol,*
505 277**,** E291-8.
506 BENITEZ, D. P., JIANG, S., WOOD, J., WANG, R., HALL, C. M., PEERBOOM, C., WONG, N., STRINGER, K. M.,
507 VITANOVA, K. S., SMITH, V. C., JOSHI, D., SAITO, T., SAIDO, T. C., HARDY, J., HANRIEDER, J., DE
508 STROOPER, B., SALIH, D. A., TRIPATHI, T., EDWARDS, F. A. & CUMMINGS, D. M. 2021. Knock-in
509 models related to Alzheimer's disease: synaptic transmission, plaques and the role of microglia.
510 *Mol Neurodegener,* 16**,** 47.
511 BERTOLIO, R., NAPOLETANO, F., MANO, M., MAURER-STROH, S., FANTUZ, M., ZANNINI, A., BICCIATO, S.,
512 SORRENTINO, G. & DEL SAL, G. 2019. Sterol regulatory element binding protein 1 couples
513 mechanical cues and lipid metabolism. *Nat Commun,* 10**,** 1326.
514 BIESSELS, G. J. & DESPA, F. 2018. Cognitive decline and dementia in diabetes mellitus: mechanisms and
515 clinical implications. *Nat Rev Endocrinol,* 14**,** 591-604.
516 BORST, S. E., CONOVER, C. F. & BAGBY, G. J. 2005. Association of resistin with visceral fat and muscle
517 insulin resistance. *Cytokine,* 32**,** 39-44.
518 BREIJYEH, Z. & KARAMAN, R. 2020. Comprehensive Review on Alzheimer's Disease: Causes and
519 Treatment. *Molecules,* 25.
520 BUDAMAGUNTA, V., KUMAR, A., RANI, A., BEAN, L., MANOHAR-SINDHU, S., YANG, Y., ZHOU, D. &
521 FOSTER, T. C. 2023. Effect of peripheral cellular senescence on brain aging and cognitive decline.
522 *Aging Cell,* 22**,** e13817.
523 CHUSYD, D. E., WANG, D., HUFFMAN, D. M. & NAGY, T. R. 2016. Relationships between Rodent White
524 Adipose Fat Pads and Human White Adipose Fat Depots. *Front Nutr,* 3**,** 10.
525 CURRAIS, A., PRIOR, M., DARGUSCH, R., ARMANDO, A., EHREN, J., SCHUBERT, D., QUEHENBERGER, O. &
526 MAHER, P. 2014. Modulation of p25 and inflammatory pathways by fisetin maintains cognitive
527 function in Alzheimer's disease transgenic mice. *Aging Cell,* 13**,** 379-90.
528 DONATO, A. J., HENSON, G. D., HART, C. R., LAYEC, G., TRINITY, J. D., BRAMWELL, R. C., ENZ, R. A.,
529 MORGAN, R. G., REIHL, K. D., HAZRA, S., WALKER, A. E., RICHARDSON, R. S. & LESNIEWSKI, L. A.
530 2014. The impact of ageing on adipose structure, function and vasculature in the B6D2F1
531 mouse: evidence of significant multisystem dysfunction. *J Physiol,* 592**,** 4083-96.
532 DOVE, A., SHANG, Y., XU, W., GRANDE, G., LAUKKA, E. J., FRATIGLIONI, L. & MARSEGLIA, A. 2021. The
533 impact of diabetes on cognitive impairment and its progression to dementia. *Alzheimers*
534 *Dement,* 17**,** 1769-1778.
535 ELIAS, M. F., ELIAS, P. K., SULLIVAN, L. M., WOLF, P. A. & D'AGOSTINO, R. B. 2005. Obesity, diabetes and
536 cognitive deficit: The Framingham Heart Study. *Neurobiol Aging,* 26 Suppl 1**,** 11-6.

FANG, Y., MCFADDEN, S., DARCY, J., HASCUP, E. R., HASCUP, K. N. & BARTKE, A. 2020. Lifespan of long-lived growth hormone receptor knockout mice was not normalized by housing at 30 degrees C since weaning. *Aging Cell,* 19**,** e13123.

FANG, Y., MEDINA, D., STOCKWELL, R., MCFADDEN, S., QUINN, K., PECK, M. R., BARTKE, A., HASCUP, K. N. & HASCUP, E. R. 2023. Sexual dimorphic metabolic and cognitive responses of C57BL/6 mice to Fisetin or Dasatinib and quercetin cocktail oral treatment. *Geroscience,* 45**,** 2835-2850.

FANG, Y., PECK, M. R., QUINN, K., CHAPMAN, J. E., MEDINA, D., MCFADDEN, S. A., BARTKE, A., HASCUP, E. R. & HASCUP, K. N. 2025. Senolytic intervention improves cognition, metabolism, and adiposity in female APP(NL)(-F/NL-F) mice. *Geroscience,* 47**,** 1123-1138.

FERNANDES, C., FORNY-GERMANO, L., ANDRADE, M. M., LYRA, E. S. N. M., RAMOS-LOBO, A. M., MEIRELES, F., TOVAR-MOLL, F., HOUZEL, J. C., DONATO, J., JR. & DE FELICE, F. G. 2024. Leptin receptor reactivation restores brain function in early-life Lepr-deficient mice. *Brain,* 147**,** 2706-2717.

FINDLEY, C. A., BARTKE, A., HASCUP, K. N. & HASCUP, E. R. 2019. Amyloid Beta-Related Alterations to Glutamate Signaling Dynamics During Alzheimer's Disease Progression. *ASN Neuro,* 11**,** 1759091419855541.

FOSTER, M. T., SHI, H., SEELEY, R. J. & WOODS, S. C. 2011. Removal of intra-abdominal visceral adipose tissue improves glucose tolerance in rats: role of hepatic triglyceride storage. *Physiol Behav,* 104**,** 845-54.

FRANCZYK, M. P., HE, M. & YOSHINO, J. 2021. Removal of Epididymal Visceral Adipose Tissue Prevents Obesity-Induced Multi-organ Insulin Resistance in Male Mice. *J Endocr Soc,* 5**,** bvab024.

GABRIELY, I., MA, X. H., YANG, X. M., ATZMON, G., RAJALA, M. W., BERG, A. H., SCHERER, P., ROSSETTI, L. & BARZILAI, N. 2002. Removal of visceral fat prevents insulin resistance and glucose intolerance of aging: an adipokine-mediated process? *Diabetes,* 51**,** 2951-8.

GUERRA, S. & GASTALDELLI, A. 2020. The role of the liver in the modulation of glucose and insulin in non alcoholic fatty liver disease and type 2 diabetes. *Curr Opin Pharmacol,* 55**,** 165-174.

GUO, D. H., YAMAMOTO, M., HERNANDEZ, C. M., KHODADADI, H., BABAN, B. & STRANAHAN, A. M. 2020. Visceral adipose NLRP3 impairs cognition in obesity via IL-1R1 on CX3CR1+ cells. *J Clin Invest,* 130**,** 1961-1976.

GUSTAFSON, D. R. 2012. Adiposity and cognitive decline: underlying mechanisms. *J Alzheimers Dis,* 30 Suppl 2**,** S97-112.

HAN, H. S., KANG, G., KIM, J. S., CHOI, B. H. & KOO, S. H. 2016. Regulation of glucose metabolism from a liver-centric perspective. *Exp Mol Med,* 48**,** e218.

HERNANDEZ, T. L., KITTELSON, J. M., LAW, C. K., KETCH, L. L., STOB, N. R., LINDSTROM, R. C., SCHERZINGER, A., STAMM, E. R. & ECKEL, R. H. 2011. Fat redistribution following suction lipectomy: defense of body fat and patterns of restoration. *Obesity (Silver Spring),* 19**,** 1388-95.

HUANG, X., WANG, Y. J. & XIANG, Y. 2022. Bidirectional communication between brain and visceral white adipose tissue: Its potential impact on Alzheimer's disease. *EBioMedicine,* 84**,** 104263.

KAMOGAWA, K., KOHARA, K., TABARA, Y., UETANI, E., NAGAI, T., YAMAMOTO, M., IGASE, M. & MIKI, T. 2010. Abdominal fat, adipose-derived hormones and mild cognitive impairment: the J-SHIPP study. *Dement Geriatr Cogn Disord,* 30**,** 432-9.

KHORAMIPOUR, K., CHAMARI, K., HEKMATIKAR, A. A., ZIYAIYAN, A., TAHERKHANI, S., ELGUINDY, N. M. & BRAGAZZI, N. L. 2021. Adiponectin: Structure, Physiological Functions, Role in Diseases, and Effects of Nutrition. *Nutrients,* 13.

KIM, S., YI, H. A., WON, K. S., LEE, J. S. & KIM, H. W. 2022. Association between Visceral Adipose Tissue Metabolism and Alzheimer's Disease Pathology. *Metabolites,* 12.

583 KIM, Y. W., KIM, J. Y. & LEE, S. K. 1999. Surgical removal of visceral fat decreases plasma free fatty acid
584 and increases insulin sensitivity on liver and peripheral tissue in monosodium glutamate (MSG)-
585 obese rats. *J Korean Med Sci,* 14**,** 539-45.
586 KOJTA, I., CHACINSKA, M. & BLACHNIO-ZABIELSKA, A. 2020. Obesity, Bioactive Lipids, and Adipose Tissue
587 Inflammation in Insulin Resistance. *Nutrients,* 12.
588 LIEB, W., BEISER, A. S., VASAN, R. S., TAN, Z. S., AU, R., HARRIS, T. B., ROUBENOFF, R., AUERBACH, S.,
589 DECARLI, C., WOLF, P. A. & SESHADRI, S. 2009. Association of plasma leptin levels with incident
590 Alzheimer disease and MRI measures of brain aging. *JAMA,* 302**,** 2565-72.
591 LING, B. L., CHIU, C. T., LU, H. C., LIN, J. J., KUO, C. Y. & CHOU, F. P. 2014. Short and long-term impact of
592 lipectomy on expression profile of hepatic anabolic genes in rats: a high fat and high cholesterol
593 diet-induced obese model. *PLoS One,* 9**,** e108717.
594 MASTERNAK, M. M., BARTKE, A., WANG, F., SPONG, A., GESING, A., FANG, Y., SALMON, A. B., HUGHES, L.
595 F., LIBERATI, T., BOPARAI, R., KOPCHICK, J. J. & WESTBROOK, R. 2012. Metabolic effects of intra-
596 abdominal fat in GHRKO mice. *Aging Cell,* 11**,** 73-81.
597 MOSER, V. A. & PIKE, C. J. 2016. Obesity and sex interact in the regulation of Alzheimer's disease.
598 *Neurosci Biobehav Rev,* 67**,** 102-18.
599 MURILLO, A. L., KAISER, K. A., SMITH, D. L., JR., PETERSON, C. M., AFFUSO, O., TIWARI, H. K. & ALLISON,
600 D. B. 2019. A Systematic Scoping Review of Surgically Manipulated Adipose Tissue and the
601 Regulation of Energetics and Body Fat in Animals. *Obesity (Silver Spring),* 27**,** 1404-1417.
602 NG, P. Y., ZHANG, C., LI, H. & BAKER, D. J. 2024. Senescence Targeting Methods Impact Alzheimer's
603 Disease Features in 3xTg Mice. *J Alzheimers Dis,* 97**,** 1751-1763.
604 NGUYEN, J. C., KILLCROSS, A. S. & JENKINS, T. A. 2014. Obesity and cognitive decline: role of
605 inflammation and vascular changes. *Front Neurosci,* 8**,** 375.
606 OH, H. S., RUTLEDGE, J., NACHUN, D., PALOVICS, R., ABIOSE, O., MORAN-LOSADA, P., CHANNAPPA, D.,
607 UREY, D. Y., KIM, K., SUNG, Y. J., WANG, L., TIMSINA, J., WESTERN, D., LIU, M., KOHLFELD, P.,
608 BUDDE, J., WILSON, E. N., GUEN, Y., MAURER, T. M., HANEY, M., YANG, A. C., HE, Z., GREICIUS,
609 M. D., ANDREASSON, K. I., SATHYAN, S., WEISS, E. F., MILMAN, S., BARZILAI, N., CRUCHAGA, C.,
610 WAGNER, A. D., MORMINO, E., LEHALLIER, B., HENDERSON, V. W., LONGO, F. M.,
611 MONTGOMERY, S. B. & WYSS-CORAY, T. 2023. Organ aging signatures in the plasma proteome
612 track health and disease. *Nature,* 624**,** 164-172.
613 PALMER, A. K., TCHKONIA, T. & KIRKLAND, J. L. 2021. Senolytics: Potential for Alleviating Diabetes and Its
614 Complications. *Endocrinology,* 162.
615 PARHOFER, K. G. 2015. Interaction between Glucose and Lipid Metabolism: More than Diabetic
616 Dyslipidemia. *Diabetes Metab J,* 39**,** 353-62.
617 PETERSEN, M. C. & SHULMAN, G. I. 2018. Mechanisms of Insulin Action and Insulin Resistance. *Physiol*
618 *Rev,* 98**,** 2133-2223.
619 PITOMBO, C., ARAUJO, E. P., DE SOUZA, C. T., PAREJA, J. C., GELONEZE, B. & VELLOSO, L. A. 2006.
620 Amelioration of diet-induced diabetes mellitus by removal of visceral fat. *J Endocrinol,* 191**,** 699-
621 706.
622 RABE, K., LEHRKE, M., PARHOFER, K. G. & BROEDL, U. C. 2008. Adipokines and insulin resistance. *Mol*
623 *Med,* 14**,** 741-51.
624 RICHARD, A. J., WHITE, U., ELKS, C. M. & STEPHENS, J. M. 2000. Adipose Tissue: Physiology to Metabolic
625 Dysfunction. *In:* FEINGOLD, K. R., AHMED, S. F., ANAWALT, B., BLACKMAN, M. R., BOYCE, A.,
626 CHROUSOS, G., CORPAS, E., DE HERDER, W. W., DHATARIYA, K., DUNGAN, K., HOFLAND, J.,
627 KALRA, S., KALTSAS, G., KAPOOR, N., KOCH, C., KOPP, P., KORBONITS, M., KOVACS, C. S.,
628 KUOHUNG, W., LAFERRERE, B., LEVY, M., MCGEE, E. A., MCLACHLAN, R., MUZUMDAR, R.,
629 PURNELL, J., REY, R., SAHAY, R., SHAH, A. S., SINGER, F., SPERLING, M. A., STRATAKIS, C. A.,
630 TRENCE, D. L. & WILSON, D. P. (eds.) *Endotext.* South Dartmouth (MA).

SAITO, T., MATSUBA, Y., MIHIRA, N., TAKANO, J., NILSSON, P., ITOHARA, S., IWATA, N. & SAIDO, T. C. 2014. Single App knock-in mouse models of Alzheimer's disease. *Nat Neurosci,* 17**,** 661-3.

SAKERS, A., DE SIQUEIRA, M. K., SEALE, P. & VILLANUEVA, C. J. 2022. Adipose-tissue plasticity in health and disease. *Cell,* 185**,** 419-446.

SCODITTI, E., SABATINI, S., CARLI, F. & GASTALDELLI, A. 2024. Hepatic glucose metabolism in the steatotic liver. *Nat Rev Gastroenterol Hepatol,* 21**,** 319-334.

SERETIS, K., GOULIS, D. G., KOLIAKOS, G. & DEMIRI, E. 2015. Short- and Long-Term Effects of Abdominal Lipectomy on Weight and Fat Mass in Females: a Systematic Review. *Obes Surg,* 25**,** 1950-8.

SETHI, J. K. & VIDAL-PUIG, A. 2005. Visfatin: the missing link between intra-abdominal obesity and diabetes? *Trends Mol Med,* 11**,** 344-7.

SHI, H., STRADER, A. D., WOODS, S. C. & SEELEY, R. J. 2007a. The effect of fat removal on glucose tolerance is depot specific in male and female mice. *Am J Physiol Endocrinol Metab,* 293**,** E1012-20.

SHI, H., STRADER, A. D., WOODS, S. C. & SEELEY, R. J. 2007b. Sexually dimorphic responses to fat loss after caloric restriction or surgical lipectomy. *Am J Physiol Endocrinol Metab,* 293**,** E316-26.

SHIN, J. A., JEONG, S. I., KIM, M., YOON, J. C., KIM, H. S. & PARK, E. M. 2015. Visceral adipose tissue inflammation is associated with age-related brain changes and ischemic brain damage in aged mice. *Brain Behav Immun,* 50**,** 221-231.

ST-ONGE, M. P. & GALLAGHER, D. 2010. Body composition changes with aging: the cause or the result of alterations in metabolic rate and macronutrient oxidation? *Nutrition,* 26**,** 152-5.

STEINER, B. M. & BERRY, D. C. 2022. The Regulation of Adipose Tissue Health by Estrogens. *Front Endocrinol (Lausanne),* 13**,** 889923.

SUN, R., HE, T., PAN, Y. & KATUSIC, Z. S. 2018. Effects of senescence and angiotensin II on expression and processing of amyloid precursor protein in human cerebral microvascular endothelial cells. *Aging (Albany NY),* 10**,** 100-114.

TCHKONIA, T., MORBECK, D. E., VON ZGLINICKI, T., VAN DEURSEN, J., LUSTGARTEN, J., SCRABLE, H., KHOSLA, S., JENSEN, M. D. & KIRKLAND, J. L. 2010. Fat tissue, aging, and cellular senescence. *Aging Cell,* 9**,** 667-84.

TRAN, T. M., DAI, T. X. T., TRAN, D. B., NGUYEN, Q. C. T. & NGUYEN, D. H. Y. 2019. A simple spectrophotometric method for quantifying total lipids in plants and animals. *CTU Journal of Innovation and Sustainable Development,* 11**,** 106-110.

VISHVANATH, L. & GUPTA, R. K. 2019. Contribution of adipogenesis to healthy adipose tissue expansion in obesity. *J Clin Invest,* 129**,** 4022-4031.

WANG, G., LI, G., SONG, A., ZHAO, Y., YU, J., WANG, Y., DAI, W., SALAS, M., QIN, H., MEDRANO, L., DOW, J., LI, A., ARMSTRONG, B., FUEGER, P. T., YU, H., ZHU, Y., SHAO, M., WU, X., JIANG, L., CAMPISI, J., YANG, X. & WANG, Q. A. 2025. Distinct adipose progenitor cells emerging with age drive active adipogenesis. *Science,* 388**,** eadj0430.

WHITMER, R. A., GUSTAFSON, D. R., BARRETT-CONNOR, E., HAAN, M. N., GUNDERSON, E. P. & YAFFE, K. 2008. Central obesity and increased risk of dementia more than three decades later. *Neurology,* 71**,** 1057-64.

WONG ZHANG, D. E., TRAN, V., VINH, A., DINH, Q. N., DRUMMOND, G. R., SOBEY, C. G., JELINIC, M. & DE SILVA, T. M. 2023. Pathophysiological Links Between Obesity and Dementia. *Neuromolecular Med,* 25**,** 451-456.

WU, Y., LEE, M. J., IDO, Y. & FRIED, S. K. 2017. High-fat diet-induced obesity regulates MMP3 to modulate depot- and sex-dependent adipose expansion in C57BL/6J mice. *Am J Physiol Endocrinol Metab,* 312**,** E58-E71.

YANAI, H. & YOSHIDA, H. 2019. Beneficial Effects of Adiponectin on Glucose and Lipid Metabolism and Atherosclerotic Progression: Mechanisms and Perspectives. *Int J Mol Sci,* 20.

679 ZHANG, P., KISHIMOTO, Y., GRAMMATIKAKIS, I., GOTTIMUKKALA, K., CUTLER, R. G., ZHANG, S.,
680 ABDELMOHSEN, K., BOHR, V. A., MISRA SEN, J., GOROSPE, M. & MATTSON, M. P. 2019. Senolytic
681 therapy alleviates Abeta-associated oligodendrocyte progenitor cell senescence and cognitive
682 deficits in an Alzheimer's disease model. *Nat Neurosci,* 22**,** 719-728.
683 ZHAO, Z., XIANG, X., CHEN, Q., DU, J., ZHU, S., XU, X., SHEN, Y., WEN, S., LI, Y., XU, W., MAI, K. & AI, Q.
684 2024. Sterol Regulatory Element Binding Protein 1: A Mediator for High-Fat Diet-Induced
685 Hepatic Gluconeogenesis and Glucose Intolerance in Fish. *J Nutr,* 154**,** 1505-1516.
686 ZHU, J., WU, C. & YANG, L. 2024. Cellular senescence in Alzheimer's disease: from physiology to
687 pathology. *Transl Neurodegener,* 13**,** 55.

688

689 **Figure Legends**

690 *Figure 1 - Novel object recognition and body composition analysis after VFR*. Retention index
691 (A) and novelty preference (B) for the NOR task. Body weight (C) and the percentage of vWAT
692 (D) and total fat mass for three adipose depots (brown, subcutaneous, and visceral; E) in
693 relation to body weight. The percentage of VFR mice that regenerated vWAT (reg. ratio) are
694 shown in (D). Data are represented as means ± SEM. *p<0.05, ***p<0.001 based on a two-
695 tailed Student's *t* test (n=9-20).

696 *Figure 2 – Lipid metabolism in hepatic and visceral white adipose tissue.* Percentage of total
697 liver lipids (A). Relative gene expression profile of lipolysis and lipogenesis genes in the liver (B)
698 and vWAT (C). Data are represented as means ± SEM. *p<0.05, **p<0.01, ***p<0.001,
699 ****p<0.0001 based on a two-tailed Student's *t* test (n=8-15). Abbreviations: ACC – acetyl CoA-
700 carboxylase, FAS – fatty acid synthase, SCD1 - stearoyl-CoA Desaturase, Elovl6 – fatty acid
701 elongase enzyme 6, SREBP1 – sterol regulator element-binding protein 1, MGL –
702 monoglyceride lipase, PKA – protein kinase A, ATGL – adipose triglyceride lipase, HSL –
703 hormone sensitive lipase

704 *Figure 3 – Blood glucose levels in pre-symptomatic and symptomatic APP^{NL-F} mice.* Glucose
705 tolerance test (GTT; A) and insulin tolerance test (ITT; B) and their respective area under the
706 curve (AUC; inset) in pre-symptomatic (left) and symptomatic (right) cohorts. Fasting (C) and
707 fed (D) blood glucose levels were determined from t=0 during the GTT and ITT, respectively.
708 Data are represented as means ± SEM. *p<0.05 based on a two-tailed Student's t test (n=9-16).

709 *Figure 4 – Liver glucose metabolism and plasma adipokines*. Hepatic relative gene expression
710 profiles (A) of gluconeogenesis (G6PC, PEPCK), glycolysis (GLUT2, GCK), and glycogenesis
711 (GYS2). Circulating visfatin (B), adiponectin (C), and Leptin (D) determined by ELISA from
712 plasma collected at the time of euthanization. Data are represented as means ± SEM. *p<0.05

713 based on a two-tailed Student's t test (n=4-12). Abbreviations: G6PC - glucose-6-phosphatase,
714 PEPCK - phosphoenolpyruvate carboxykinase, Glut2 - glucose transporter 2, GCK -
715 glucokinase, GYS2 - glycogen synthase 2 (GYS2)

716 *Figure 5 – Senescent cell and inflammation markers in visceral and subcutaneous white*
717 *adipose tissue.* Visceral (A) and subcutaneous white adipose tissue (SubQ; B) relative gene
718 expression profiles of senescence ($p16^{Ink4\alpha}$, $p21^{Cip1}$) and inflammation (TNFα, IL-10, IL-6,
719 MCP1). Data are represented as means ± SEM. *p<0.05, **p<0.01, ***p<0.001 based on a two-
720 tailed Student's t test (n=4-12). Abbreviations: TNFα – tumor necrosis factor alpha, IL –
721 interleukin, MCP1 – monocyte chemoattractant protein 1.

722 Figure 6 - *Senescent cell and inflammation markers in the hippocampus.* Hippocampal relative
723 gene expression profiles (A) of senescence ($p16^{Ink4\alpha}$, $p21^{Cip1}$), inflammation (TNFα), and
724 memory (AdipoR, LepR, Creb1, PRGN) and soluble $A\beta_{42}$ (B) as determined by ELISA. Data are
725 represented as means ± SEM. *p<0.05, **p<0.01, ***p<0.001 based on a two-tailed Student's t
726 test (n=4-12). Abbreviations: TNFα – tumor necrosis factor alpha, AdipoR – adiponectin
727 receptor, LepR – leptin receptor, Creb1 – cyclic AMP Response Element-Binding Protein 1.

728

Table 1: A list of forward and reverse primers. The last gene listed for each tissue type was used as that tissue's housekeeping gene.

Gene Name (Abbreviation)	Forward Primer	Reverse Primer
Liver		
Acetyl-CoA Carboxylase (ACC)	5'-ATGGGCGGAATGGTCTCTTTC-3'	5'-TGGGGACCTTGTCTTCATCAT-3'
Fatty Acid Synthase (FAS)	5'-GGAGGTGGTGATAGCCGGTAT-3'	5'-TGGGTAATCCATAGAGCCCAG-3'
Stearoyl-CoA Desaturase (SCD1)	5'-TTCTTGCGATACACTCTGGTGC-3'	5'-CGGGATTGAATGTTCTTGTCGT-3'
Fatty Acid Elongase Enzyme 6 (Elovl6)	5'-GAAAAGCAGTTCAACGAGAACG-3'	5'-AGATGCCGACCACCAAAGATA-3'
Sterol Regulator Element-Binding Protein 1 (SREBP1)	5'-GATGTGCGAACTGGACACAG-3'	5'-CATAGGGGGCGTCAAACAG-3'
Monoglyceride Lipase (MGL)	5'-CGGACTTCCAAGTTTTTGTCAGA-	5'-GCAGCCACTAGGATGGAGATG-3'
Glucose-6-Phosphatase (G6PC)	5'-CGACTCGCTATCTCCAAGTGA-3'	5'-GTTGAACCAGTCTCCGACCA-3'
Phosphoenolpyruvate Carboxykinase (PEPCK)	5'-CTGCATAACGGTCTGGACTTC-3'	5'-CAGCAACTGCCCGTACTCC-3'
Glucose Transporter 2 (GLUT2)	5'-TCAGAAGACAAGATCACCGGA-3'	5'-GCTGGTGTGACTGTAAGTGGG-3'
Glucokinase (GLK)	5'-TGAGCCGGATGCAGAAGGA-3'	5'-GCAACATCTTTACACTGGCCT-3'
Glycogen Synthase (GYS2)	5'-ACCAAGGCCAAAACGACAG-3'	5'-GGGCTCACATTGTTCTACTTGA-3'
Beta-2 Microglobulin (BDM)	5'-AAGTATACTCACGCCACCCA-3'	5'-AGGACCAGTCCTTGCTGAAG-3'
Visceral White Adipose Tissue		
Acetyl-CoA Carboxylase (ACC)	5'-ATGGGCGGAATGGTCTCTTTC-3'	5'-TGGGGACCTTGTCTTCATCAT-3'
Fatty Acid Synthase (FAS)	5'-GGAGGTGGTGATAGCCGGTAT-3'	5'-TGGGTAATCCATAGAGCCCAG-3'
Protein Kinase A (PKA)	5'-AGATCGTCCTGACCTTTGAGT-3'	5'-GGCAAAACCGAAGTCTGTCAC-3'
Adipose Triglyceride Lipase (ATGL)	5'-GGATGGCGGCATTTCAGACA-3'	5'-CAAAGGGTTGGGTTGGTTCAG-3'
Hormone Sensitive Lipase (HSL)	5'-CCAGCCTGAGGGCTTACTG-3'	5'-CTCCATTGACTGTGACATCTCG-3'
Sterol Regulator Element-Binding Protein 1 (SREBP1)	5'-GATGTGCGAACTGGACACAG-3'	5'-CATAGGGGGCGTCAAACAG-3'
$p16^{Ink4\alpha}$	5'-CGGTCGTACCCCGATTCAG-3'	5'-GCACCGTAGTTGAGCAGAAGA-3'
$p21^{Cip1}$	5'-CCTGGTGATGTCCGACCTG-3'	5'-CCATGAGCGCATCGCAATC-3'
Tumor Necrosis Factor α (TNFα)	5'-CAGGCGGTGCCTATGTCTC-3'	5'-CGATCACCCCGAAGTTCAGTAG-3'
Interleukin-10 (IL-10)	5'-GCTCTTACTGACTGGCATGAG-3'	5'-CGCAGCTCTAGGAGCATGTG-3'
Glyceraldehyde-3-Phosphate Dehydrogenase (GAPDH)	5'-AGGTCGGTGTGAACGGATTTG-3'	5'-TGTAGACCATGTAGTTGAGGTCA-3'
Subcutaneous White Adipose Tissue		
Tumor Necrosis Factor α (TNFα)	5'-CAGGCGGTGCCTATGTCTC-3'	5'-CGATCACCCCGAAGTTCAGTAG-3'

Interleukin-10 (IL-10)	5'-GCTCTTACTGACTGGCATGAG-3'	5'-CGCAGCTCTAGGAGCATGTG-3'
Interleukin-6 (IL-6)	5'-CTGCAAGAGACTTCCATCCAG-3'	5'-AGTGGTATAGACAGGTCTGTTGG-3'
Monocyte Chemoattractant Protein-1 (MCP1)	5'-CCACTCACCTGCTGCTACTCAT-3'	5'-TGGTGATCCTCTTGTAGCTCTCC-3'
Beta-2 Microglobulin (BDM)	5'-AAGTATACTCACGCCACCCA-3'	5'-AGGACCAGTCCTTGCTGAAG-3'
Hippocampus		
$p16^{Ink4\alpha}$	5'-CGGTCGTACCCCGATTCAG-3'	5'-GCACCGTAGTTGAGCAGAAGA-3'
$p21^{Cip1}$	5'-CCTGGTGATGTCCGACCTG-3'	5'-CCATGAGCGCATCGCAATC-3'
Tumor Necrosis Factor α (TNFα)	5'-CAGGCGGTGCCTATGTCTC-3'	5'-CGATCACCCCGAAGTTCAGTAG-3'
Adiponectin Receptor 1 (AdipoR1)	5'-TCTTCGGGATGTTCTTCCTGG-3'	5'-TTTGGAAAAAGTCCGAGAGACC-3'
cAMP Response Element-Binding Protein 1 (CREB1)	5'-CCCAAAAACGAAGGGAAATCCT-3'	5'-CCTGGTGCATCAGAAGATAAGTC-3'
Leptin Receptor (LEPR)	5'-TGGTCCCAGCAGCTATGGT-3'	5'-ACCCAGAGAAGTTAGCACTGT-3'
Progranulin (PGRN)	5'-ATGTGGGTCCTGATGAGCTG-3'	5'-GCTCGTTATTCTAGGCCATGTG-3'
Ubiquitin Conjugating Enzyme E2 D2 (UBE2D2	5'-TGCCTGAGATTGCTCGGATCT-3'	5'-TCGCATACTTCTGAGTCCATTCC-3'

Figure 1

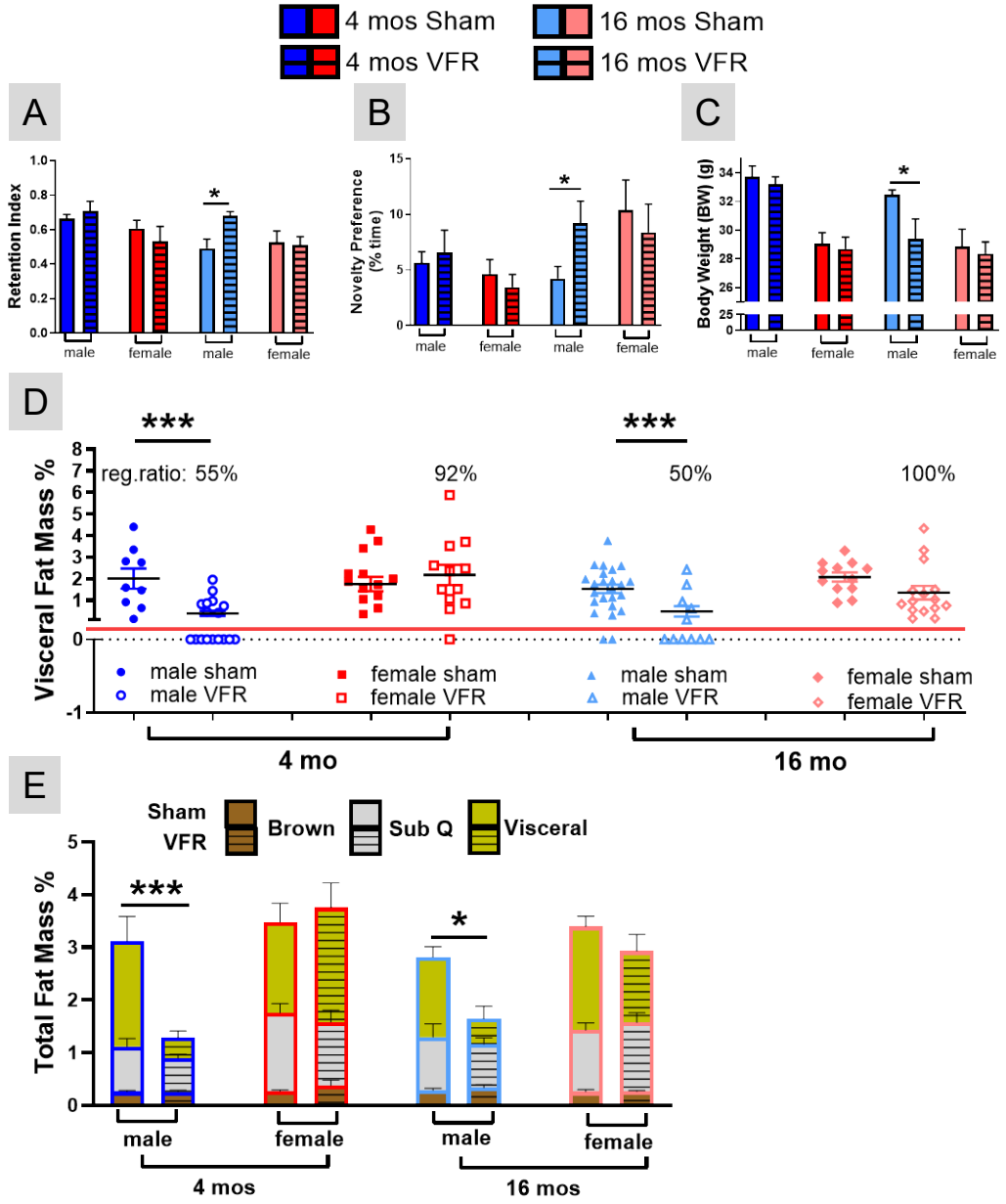
4 mos Sham
4 mos VFR
16 mos Sham
16 mos VFR
A
Retention Index
male
female
male
female
B
Novelty Preference (% time)
male
female
male
female
C
Body Weight (BW) (g)
male
female
male
female
D
Visceral Fat Mass %
reg.ratio: 55%
92%
50%
100%
male sham
male VFR
female sham
female VFR
male sham
male VFR
female sham
female VFR
4 mo
16 mo
E
Sham
VFR
Brown
Sub Q
Visceral
Total Fat Mass %
male
female
male
female
4 mos
16 mos

Figure 2

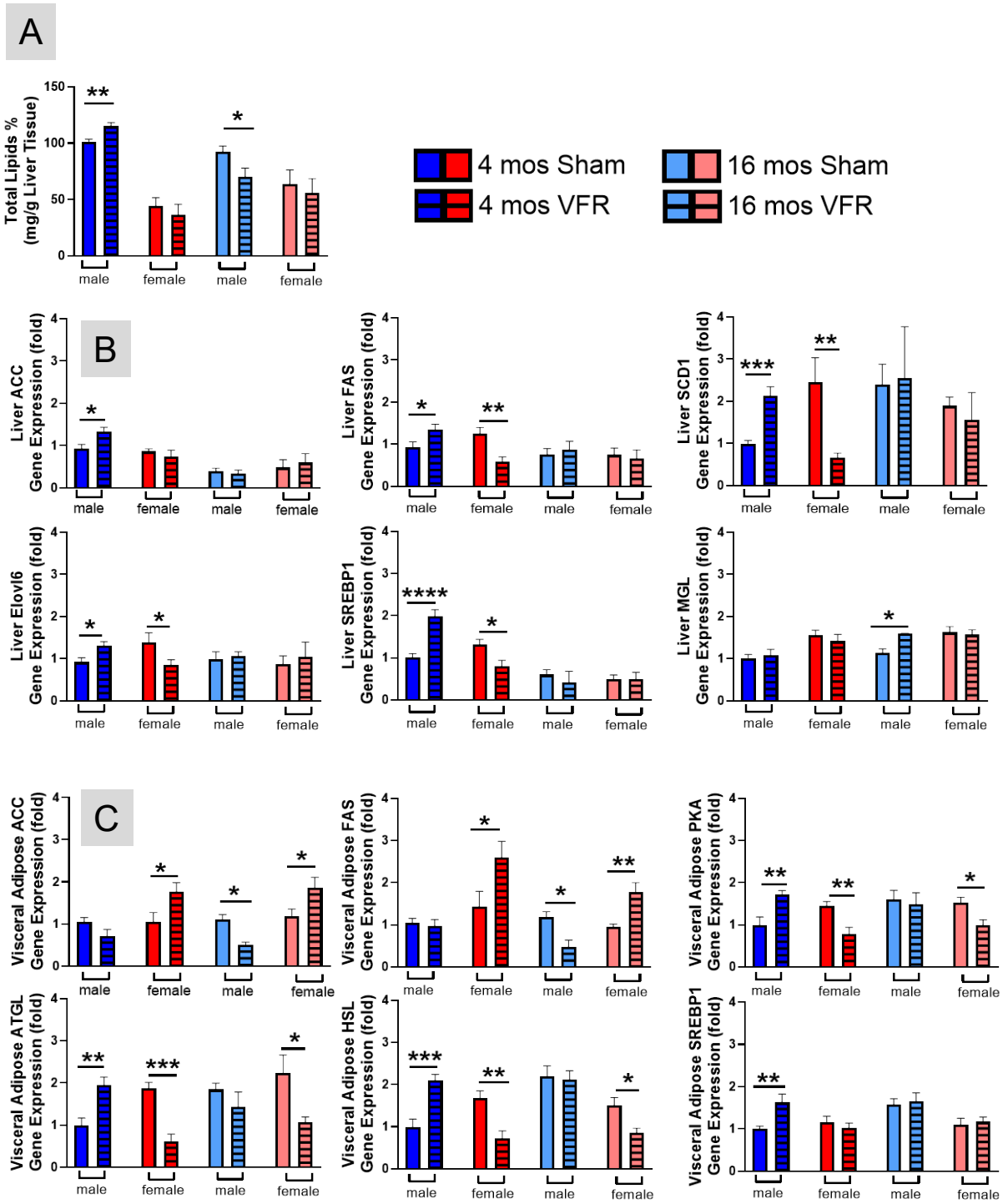
A
Total Lipids %
(mg/g Liver Tissue)
4 mos Sham
4 mos VFR
16 mos Sham
16 mos VFR
B
Liver ACC
Gene Expression (fold)
Liver FAS
Gene Expression (fold)
Liver SCD1
Gene Expression (fold)
Liver Elovl6
Gene Expression (fold)
Liver SREBP1
Gene Expression (fold)
Liver MGL
Gene Expression (fold)
C
Visceral Adipose ACC
Gene Expression (fold)
Visceral Adipose FAS
Gene Expression (fold)
Visceral Adipose PKA
Gene Expression (fold)
Visceral Adipose ATGL
Gene Expression (fold)
Visceral Adipose HSL
Gene Expression (fold)
Visceral Adipose SREBP1
Gene Expression (fold)
male
female

Figure 3

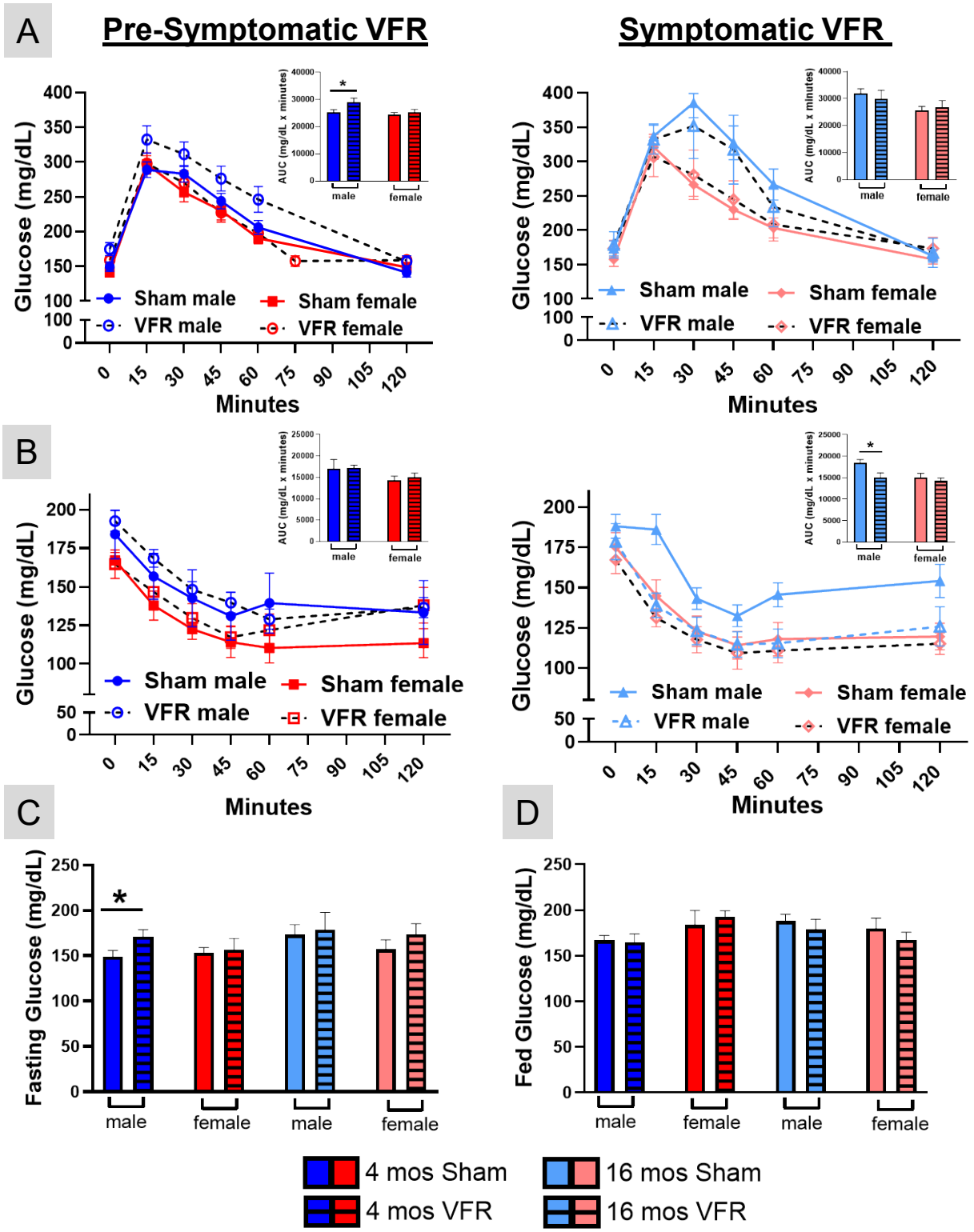
A
Pre-Symptomatic VFR
Symptomatic VFR
Glucose (mg/dL)
Minutes
Sham male
Sham female
VFR male
VFR female
AUC (mg/dL x minutes)
male
female
B
C
Fasting Glucose (mg/dL)
D
Fed Glucose (mg/dL)
4 mos Sham
4 mos VFR
16 mos Sham
16 mos VFR

Figure 4

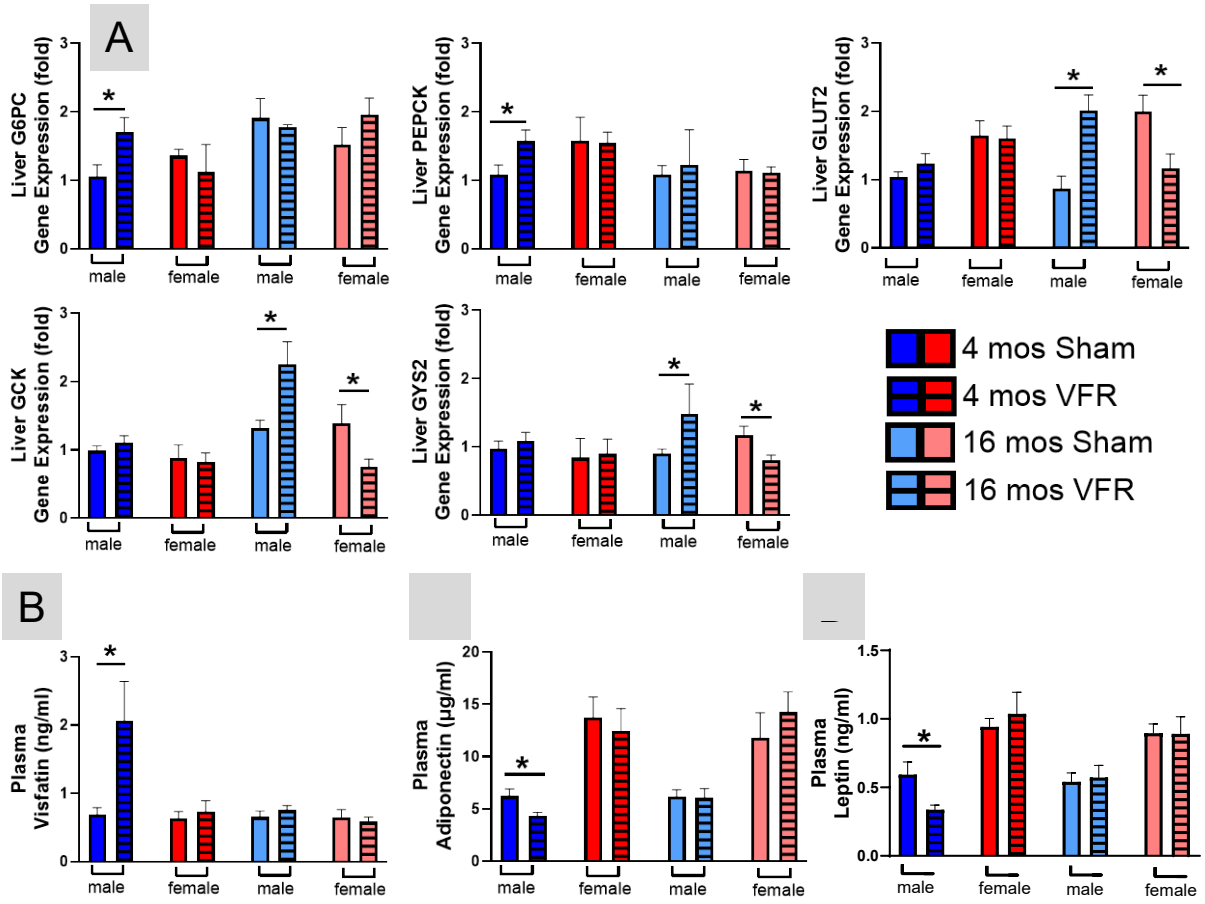
A
Liver G6PC Gene Expression (fold)
Liver PEPCK Gene Expression (fold)
Liver GLUT2 Gene Expression (fold)
Liver GCK Gene Expression (fold)
Liver GYS2 Gene Expression (fold)
male
female
4 mos Sham
4 mos VFR
16 mos Sham
16 mos VFR
B
Plasma Visfatin (ng/ml)
Plasma Adiponectin (µg/ml)
Plasma Leptin (ng/ml)

Figure 5

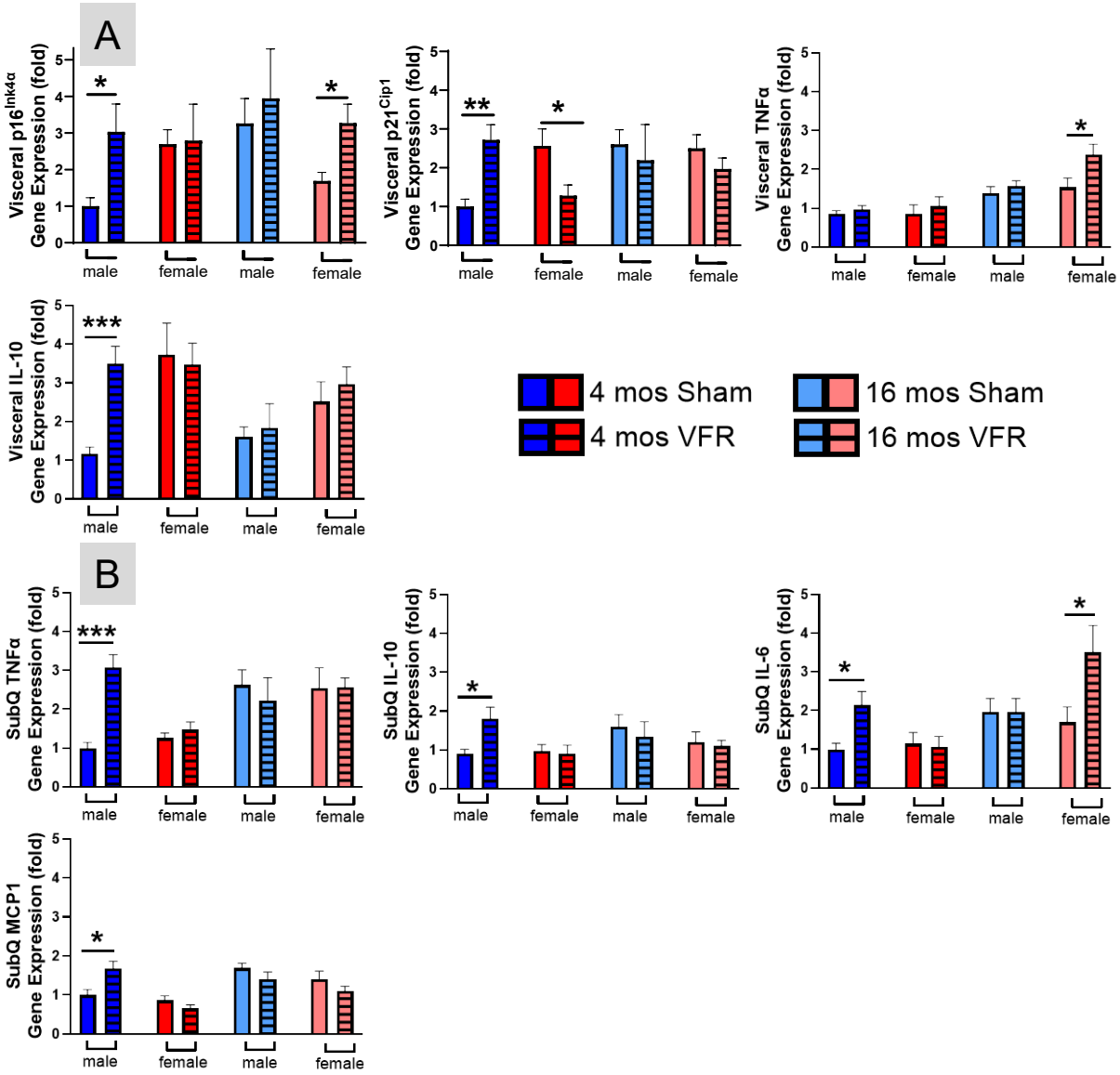
A
Visceral p16Ink4α Gene Expression (fold)
Visceral p21Cip1 Gene Expression (fold)
Visceral TNFα Gene Expression (fold)
Visceral IL-10 Gene Expression (fold)
4 mos Sham
4 mos VFR
16 mos Sham
16 mos VFR
B
SubQ TNFα Gene Expression (fold)
SubQ IL-10 Gene Expression (fold)
SubQ IL-6 Gene Expression (fold)
SubQ MCP1 Gene Expression (fold)
male
female

Figure 6

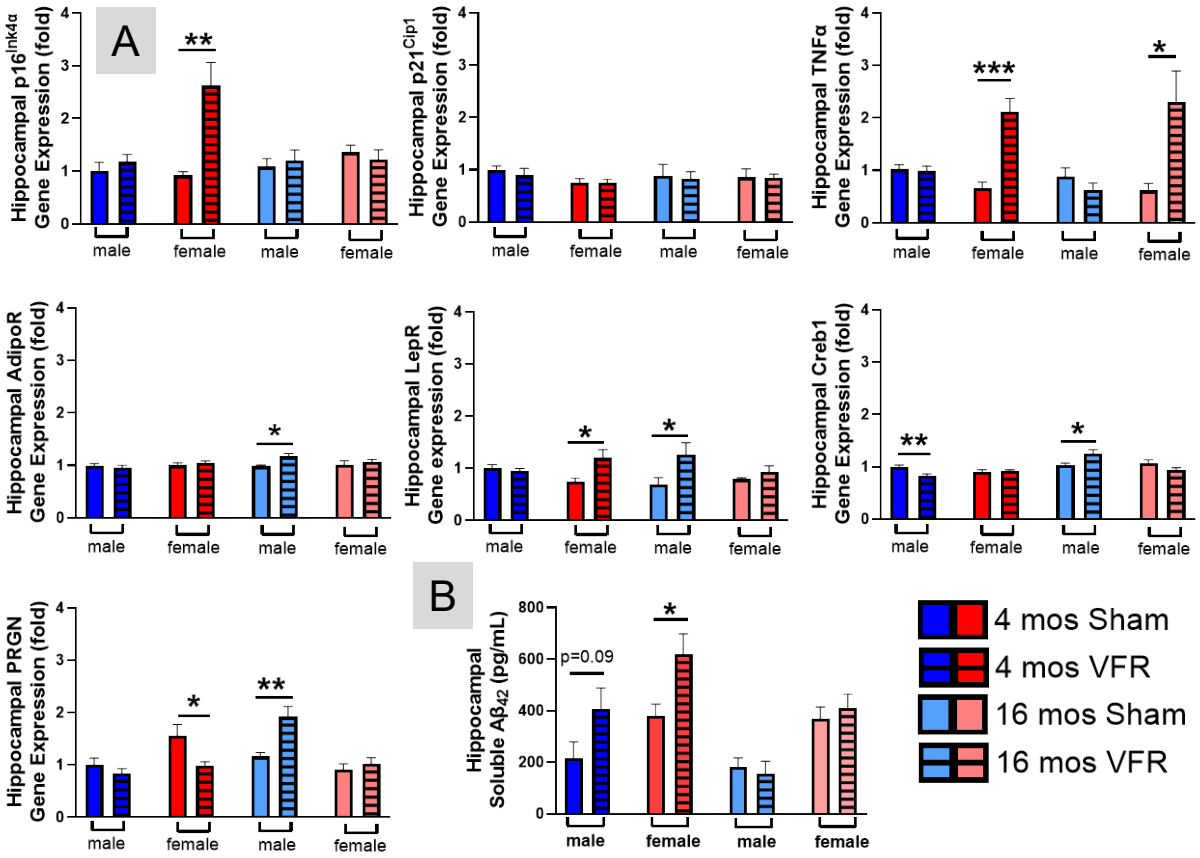
A
Hippocampal p16Ink4α Gene Expression (fold)
Hippocampal p21Cip1 Gene Expression (fold)
Hippocampal TNFα Gene Expression (fold)
Hippocampal AdipoR Gene Expression (fold)
Hippocampal LepR Gene expression (fold)
Hippocampal Creb1 Gene Expression (fold)
Hippocampal PRGN Gene Expression (fold)
B
Hippocampal Soluble Aβ42 (pg/mL)
p=0.09
male
female
4 mos Sham
4 mos VFR
16 mos Sham
16 mos VFR